THE INFLUENCE OF NANOFLUID PH ON NATURAL CONVECTION

Kouloulias K.*, Sergis A., Hardalupas Y.
*Author for correspondence
Department of Mechanical Engineering,
Imperial College London,
London SW7 2AZ
UK,
E-mail: k.kouloulias13@imperial.ac.uk

ABSTRACT

The vast majority of experimental studies of nanofluids under natural convection have shown that the heat transfer rate decreases in contrast to observations of increased heat transfer rate for forced convection and boiling heat transfer. This surprising result has not been fully understood and the purpose of this study is to shed light on the physics behind the decrease of heat transfer in Al_2O_3 – deionised (DI) H_2O nanofluids under natural convection. A classical Rayleigh-Benard configuration has been employed, where the test medium is heated from the bottom and cooled from the top of an optically accessible chamber, while the sidewalls are insulated. Al_2O_3 – H_2O nanofluids with nanoparticle concentration within the range of 0.03 to 0.12 vol. % are used and tested under turbulent natural convection, Rayleigh number Ra ~ 10^9, until steady state conditions are reached. For the synthesis of the nanofluid, pure DI water and high purity nanopowder, supplied by two different vendors, are involved with and without adopting the electrostatic stabilization method. The temperature measurements at different locations around the chamber allow the quantification of the natural convection heat transfer coefficient and the corresponding Nusselt and Rayleigh numbers. All the measured quantities are compared with those for DI water that serves as a benchmark in this study. It is found that the presence of nanoparticles systematically decreases the heat transfer performance of the base fluid under natural convection. An explanation for the reported degradation can be attributed to the buoyant and gravitational forces acting in the system that appear to be inadequate to ensure or maintain good nanofluid mixing. The results also show that as the nanoparticle concentration increases, the temperature of the heating plate increases, suggesting the presence of an additional thermal barrier imposed at the hot plate of the chamber. This can be attributed to the formation of a stationary thin layer structure of nanoparticles and liquid close to the heating plate that is qualitatively observed to increase in thickness as the nanoparticle concentration increases. The addition of a small amount of acetic acid to control the pH value of the nanofluid reduces the thickness of the thin layer structure close to the hot plate, leading to reduction of the rate of heat transfer decrease. A similar behaviour is observed when a different nanopowder that forms an acidic suspension is used. This behaviour is credited to the significantly increased nanofluid stability attained through the electrostatic stabilization method. Such a method takes advantage of the repulsive forces imposed due to the electric double layers that surround individual nanoparticles. The understanding of the influence of the nanofluid pH on the stability of nanosuspensions and its impact on heat transfer rate can lead to future guidelines for the effective use of nanofluids.

NOMENCLATURE

q''	[W/m^2]	Applied heat flux
A	[m^2]	Surface area of the heating plate
c_p	[J/KgK]	Specific heat capacity
d	[m]	Distance
F	[W]	Power output from the heat exchanger
g	[m/s^2]	Gravitational acceleration
Gr	[-]	Grashof number
h	[W/m^{2}K]	Heat transfer coefficient
k	[W/mK]	Thermal conductivity
L	[m]	Characteristic length
Nu	[-]	Nusselt number
P	[W]	Heat losses from the chamber
Pr	[-]	Prandtl number
Q	[W]	Power input from the heating plate
Ra	[-]	Rayleigh number
T	[K]	Temperature
W	[L/min]	Flow rate of cooling water

Greek characters

α	[m^2/s]	Thermal diffusivity
β	[1/K]	Thermal expansion coefficient
μ	[Ns/m^2]	Dynamic viscosity
ν	[m^2/s]	Kinematic viscosity
ρ	[kg/m^3]	Density
σ	[W/m^{2}K]	Uncertainty in the mean value of h
φ	[-]	Nanoparticle volume fraction

Subscripts

c	Cold
cl	Lower surface of the cold plate
h	Hot
hu	Upper surface of the hot plate
n	Nanoparticles
nf	Nanofluid
pl	Aluminum plate
pth	Thermocouple position
w	DI water

INTRODUCTION

Nowadays, ultra cooling performance is eagerly required by the cutting-edge industrial technology, including many engineering applications. An example is the nuclear energy

sector, where high heat fluxes, up to 20-30 MW/m^2, are present at current experimental fusion reactors and future Fusion power plants [1]. Considering this, a new approach for effective cooling needs to be followed, by involving new coolants with superior thermal characteristics.

Nanofluids, as a new category of coolants, exhibit remarkably enhanced thermal properties compared to traditional fluids. By definition, nanofluids are a new class of heat transfer fluids engineered by dispersing and stably suspending nanoparticles with typical size of the order of 1-100 nm in fluids [2], such as water, ethylene glycol or engine oil. Common materials used for nanoparticles include metals, metal oxides and carbon nanotubes [3] of volumetric fractions usually between 0.0001 and 10 % [4]. Based on a statistical analysis of the data in the literature, nanofluids offer significant enhancement for conduction, mixed conduction/convection, pool boiling and critical heat flux [4]. However, poor understanding of the physics that govern nanofluids has led to increased controversy and inconsistency among the studies [5], even when the same heat transfer mode is concerned. For instance, while for forced convection substantial heat transfer enhancement is reported [6-8], for natural convection the experimental results indicate heat transfer decrease [9-13]. However, this comes in contrast to the theoretical and numerical studies for natural convection, where heat transfer enhancement is reported [14-17]. As a consequence, additional research is required to identify the reasons behind the initially unexpected discrepancy among the studies, especially for natural convection that is widely involved in cooling applications. In low-velocity applications, such as in natural convection, nanofluid stability is of great importance. Up to date, there are three widely applied methods for the preparation of stable suspensions; the ultrasonic vibration, the electrostatic stabilisation and the steric stabilisation [18-20]. However, concerning the last two methods, they have been reported to affect the thermophysical properties of the suspension [21]. Wen and Ding [22] indicated that the addition of sodium dodecyl benzene sulfonate (SDBS) in carbon nanotubes caused severe nanofluid stability deterioration at 69 °C. Also, Eastman et al. [23] reported that in samples where a small amount of thioglycolic acid (< 1 vol. %) was added, the thermal conductivity was improved compared to non-acid-containing nanofluids.

The critical effect of the pH of the base fluid and the subsequent stability of the nanofluid has been reported in many studies in the literature [22, 24-28]. In aqueous media, the pH of a suspension is one of the most important factors that affect its zeta potential (electrophoretic mobility), the magnitude of which is an indication of the potential stability of a suspension. Nanoparticles with large negative or positive zeta potential tend to repel each other and thus eliminate their tendency to come together. For instance, a suspension with zeta potential below 20 mV exhibits limited stability, whereas for 30 mV and above, it is physically stable [29]. During the electrostatic stabilization method, ions are being absorbed by the electrophilic surface of the nanoparticles, which are dispersed in the base fluid and thus they become charged. In such a case, the net charge of the particle surface affects the distribution of ions in the surrounding interfacial region and thus an increased concentration of counter ions takes place close to the surface. As a consequence, an electrical double layer is formed around each nanoparticle that results in strong Coulomb repulsive forces among them [22, 27]. In order for the electrostatic stabilization method to be effective, the pH of the suspension has to be away from its isoelectric point (IEP), an equipotential point where the electric charge on the surface of the nanoparticles is zero [18, 30]. The IEP depends on the ionic constitution of the base fluid as well as on the material, phase and purity of the nanoparticles involved. For instance, for nanofluids containing α-Al_2O_3 nanoparticles the IEP was found to be 9.1 [26], where for γ-Al_2O_3 the IEP is between 7.7 and 7.9 [28]. Mukherjee and Paria [27] in their review for the preparation and stability of nanofluids reported that a suitable pH for alumina nanoparticles dispersed in water is around 8, compared to 9.5 and 2 for copper and graphite respectively. Wen and Ding [22] in their experimental investigation adjusted the pH of their γ-alumina nanofluid to 7, so that it would be reasonably away from the IEP and at the same time no damage would be caused to the heating surface of their apparatus. Mao et al [24] noted that when the pH was less than 7, the stability was improved, but for higher values sedimentation appeared in the system. Singh et al. [26] investigated the stability of alumina particles and found that the nanoparticles were optimally dispersed at a pH value between 3 and 7.8. As expected, they reported that as the pH approached the IEP of alumina, the stability of the nanofluid decreased.

EXPERIMENTAL FACILITY AND PROCEDURE

A. Experimental setup and controls

The setup of the experimental facility allows accurate calculations of the natural convective heat transfer coefficient in a classical Rayleigh-Benard configuration, with a volumetric capacity of 1 x 10^{-3} m^3 (1 L) and optical access through the side walls. A schematic diagram of the apparatus is illustrated in Figure 1 with all the major components clearly depicted. Following a bottom-up approach of the rig, an aluminum heating pan A of thickness 20 mm can be seen, which houses 5 parallel cartridge heaters of 1500 W power output in total. The heating pan A provides heat power to an insulating pan B that is placed on top and under the aluminum heating plate C. By this configuration, any heat transfer from the heating plate in the downward direction is eliminated. The heating plate C, providing the power input to the cell, is 25 mm thick and consists of 4 parallel cartridge heaters of 320 W power output in total. Surrounding plate C is a Teflon plate D to minimise the heat losses from the sides. The aluminum cubic cell E, where the test fluid is poured into, provides perimetric optical access for visualization studies by incorporating four quartz windows (2 large square windows of 40 mm x 40 mm in size and 2 smaller rectangular windows of 10 mm x 40 mm in size). Around this cell, there are 4 insulating pans F, 34 mm thick, and a transparent Plexiglas cover G of 10 mm thickness, for extra insulation. Finally, at the top of the test cell, there is an aluminum heat sink H connected to a cooling water supply and

a Teflon plate I, to prevent the thermal connection of the cell with the heat sink.

The experimental apparatus contains eleven thermocouples to monitor the temperature across the cooling unit, the chamber and the heating plates. More specifically, two thermocouples measure the inlet and outlet temperature of the cooling water inside the heat sink. Four thermocouples measure the temperature at the top, cold plate, 5 mm above the free surface of the cell. One thermocouple measures the temperature Th of the bottom, hot plate, 6 mm below the cell's free surface and another one measures the temperature at the bottom of the heating plate. A single thermocouple is attached to the top surface of the heating pan that provides feedback information in setting the required heat flux. Finally, two thermocouples are embedded inside the heating plate and pan to identify and prevent any overheating or failure of the cartridge heaters housed inside.

Apart from the Rayleigh-Benard cell which is the major component in this experiment, supplementary hardware, National Instruments (NI) and in-house, is installed that enables the safe operation of the chamber and provides flexibility over its control. In addition, the operation of the experimental apparatus is monitored and controlled in real time through LabVIEW software. The data, namely input heat fluxes, temperatures and power losses, are recorded with a sampling frequency of 1 Hz. The NI hardware consists of a CompactDAQ chassis (cDAQ-9188) that embodies voltage input module (NI 9213) for the temperature measurements and voltage output module (NI 9263) for the power output of the heaters assembly. The additional custom made electrical device incorporates two power controlling thyristors (United Automation PR1-DIN-2.5KW) along with two temperature controllers (TC Direct 309100). Each thyristor connects a heater assembly with the NI voltage output module, while the temperature controllers are connected with the two thermocouples that are located inside the heating pan and plate. An auto-tuning algorithm achieves fast and stable heat flux and temperature response control according to the selected boundary conditions.

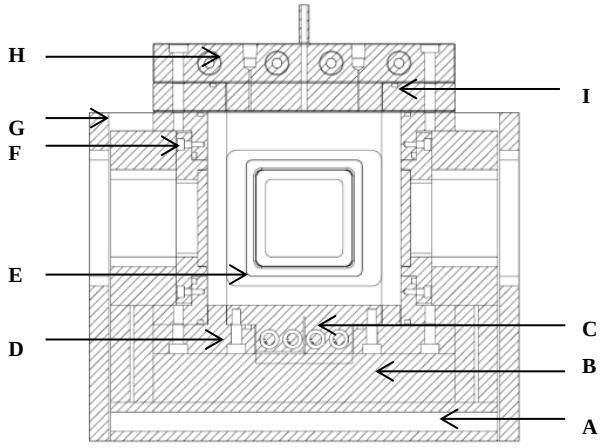

Figure 1. Schematic drawing of the natural convection chamber. The marked components are explained in the text.

B. Nanofluid preparation

A two-step preparation method was followed according to which the nanoparticles, as dry powder, are dispersed into the carrier fluid, in this study high purity deionised (DI) water. As a first step of the preparation process, the required amount of nanoparticles was measured by weight, using a high accuracy electronic balance (Sartorius semi-microbalance R 200 D). Subsequently, the nanoparticles were added to 15 ml glass test tubes and filled up with DI water. In the next step, the samples were ultrasonicated for a period of 5.0 hrs [29, 31], by employing an ultrasonic bath (Pulsatron KC2 by Guyson International Ltd). This step was necessary, since the supplied powder is initially in agglomerated form due to the strong Van der Waals attractive forces among the nanoparticles [22, 30, 32]. In addition to the ultrasonication, an analogue vortex mixer (mini vortex mixer supplied by VWR) was used to effectively break and disperse the agglomerates by inducing high shear stress in the sample.

For this study, two high purity nanopowders, supplied by two different vendors were employed for the synthesis of nanofluids. In total, three different $Al_2O_3 - H_2O$ nanofluids of various nanoparticle concentrations were prepared and compared in terms of heat transfer performance. The first sample, A, was synthesised with γ-Al_2O_3 nanoparticles, with nominal particle size less than 50 nm (quantified by TEM) and a particle density of 4000 kg/m^3, supplied by Sigma Aldrich (544833). For the second sample, B, the same nanopowder along with acetic acid (Sigma Aldrich 33209), as a pH changer added in the base fluid was used. Finally, for the third sample, C, 70:30 δ:γ-Al_2O_3 nanoparticles, supplied by Alfa Aesar (44931), with an average particle size of 45 nm (quantified by TEM) and a particle density of 3965 kg/m^3 was used. Additional TEM measurements were performed in-house for both nanopowders to verify their average particle size, shape and purity. For these measurements, a JEOL 2100F TEM operating at 200 kV was employed, according to the process described in the study of Barrett et al. [31]. Figure 2 presents TEM images for both nanopowders. It can be clearly noticed that Sigma Aldrich nanoparticles are highly agglomerated and form large clusters. Concerning their shape and average size, they look like nanoclay flakes with an average diameter of 10 nm. The Alfa Aesar particles are spherical in shape with an average diameter of 50 nm. In Figure 3, the spectral data for the two nanopowders is presented, verifying the high purity (> 99 %) of both powders.

(a)

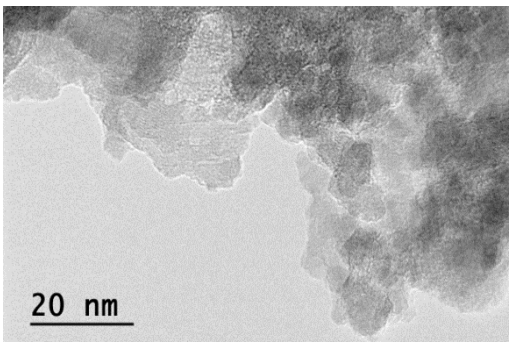

(b)

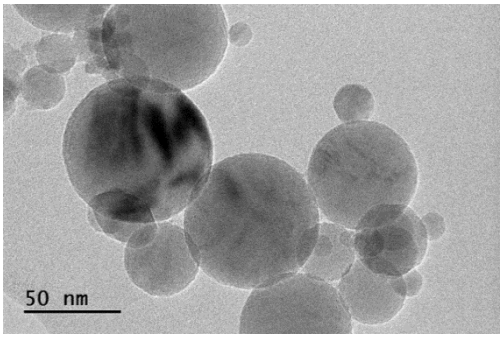

Figure 2. TEM images of Al_2O_3 nanoparticles, revealing the average particle size and shape for the (a) A, B samples and (b) C sample.

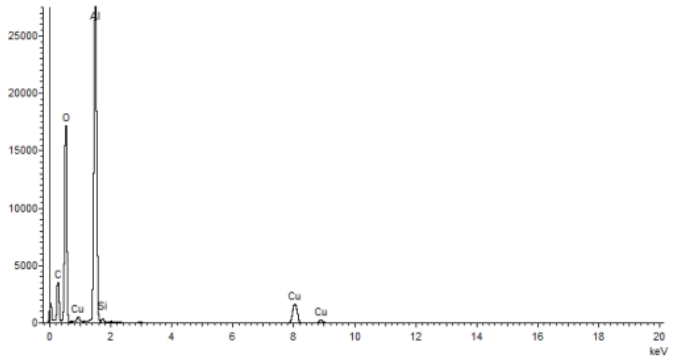

(a)

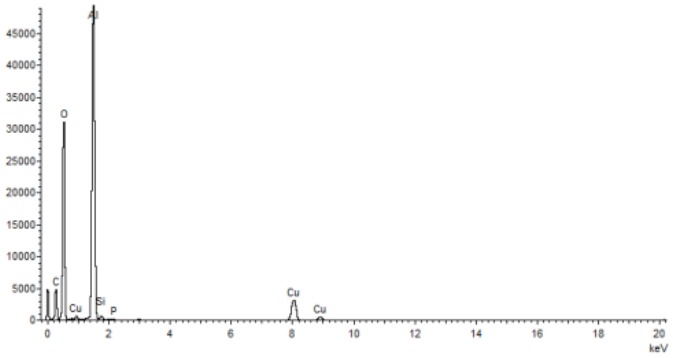

(b)

Figure 3. TEM spectral data revealing highly pure aluminum oxide powder with minor impurities in the nanopowder used for the (a) A, B samples and (b) C sample.

C. Methodology

This study was performed under high turbulent natural convective flow for all three nanofluids. The power from the heating plate was set at 125 W, which corresponds to a heat flux of 19531.3 W/m^2 with minor heat losses from the chamber, less than 5 % of the input heat flux. Al_2O_3 – DI H_2O nanofluids of various concentrations, ranging from 0.03 to 0.12 vol. % were synthesized and tested under steady state conditions. In order to eliminate any issues related to the stability of the suspension, the nanofluid experiments were performed as soon as steady state conditions for pure DI water had been reached. During the transition from DI water to nanofluid, the heaters were deactivated for a short period of time (~5 min) and the top, cold plate was removed. Then, the sonicated nanofluid samples were poured into the chamber and stirred well with the rest of the base fluid to ensure good dispersion. Subsequently, the heating elements were switched on again and the rig was operated until steady state conditions were reached. At steady state, the temperatures at the hot and cold plate were obtained by averaging a sample of 1000 measurements recorded with a sampling frequency of 1 Hz; this ensures that the effect of temperature fluctuations due to the turbulent flow is eliminated. Then, the heat transfer properties, namely heat transfer coefficient, Nusselt and Rayleigh numbers were calculated. Finally, the values presented for DI water and used for comparison are average values from a total of nine runs.

D. Repeatability test and error analysis

To ensure reliability of the results and to identify any systematic uncertainties induced either by the experimental process or by the nanofluid preparation method, repeatability tests were performed. As a result, depending on the uncertainty of the calculated values, the precision of the experiments was defined. Concerning the uncertainty in the mean value of the heat transfer coefficient, it was calculated according to Kirkup [33] and found to be negligibly small. More specifically, for DI water, σ_w was found to be 2 W/m^{2}K. For the nanofluid, due to time and cost limitations, a single repeatability test was performed for an arbitrary selected nanofluid. Thus, from a set of five individual measurements for an Al_2O_3 – H_2O nanofluid with a nanoparticle concentration of 0.03 vol. %, the uncertainty in the mean value, σ_{nf} was also found to be 2 W/m^{2}K. Regarding the determination of the uncertainty in the individual values that characterize the thermal performance of the test liquids, this was done through error propagation. Main sources of uncertainty in the calculations were the resolution of the flow meter before the flow inlet of the heat sink, ± 0.055 L/min, the tolerance of the thermocouples, ± 1.1 °C of the reading value and the measurement error of the control instrumentation, ± 0.9 °C for the temperature range of interest. In this study, where simple arithmetic calculations were required, the average uncertainty in the heat losses, from the sides of the rig, for instance, were calculated by,

$$\Delta(P) = \Delta(F) = \left|\frac{\partial F}{\partial W}\right| \Delta(W) + \left|\frac{\partial F}{\partial T}\right| \Delta(T) \quad (1)$$

where it was found to be 7.1 W. In a similar way, the mean and the maximum fractional uncertainty (%) of the heat transfer coefficient were 7.5 % and 7.9 % respectively.

RESULTS AND DISCUSSION

In this part, the heat transfer performance under natural convection for three different Al_2O_3 – H_2O nanofluids is presented and compared under fixed boundary conditions.

More specifically, the heat transfer coefficient as a function of the nanoparticle volume fraction is presented to verify the impact of nanoparticle addition to the base fluid. In addition, the relationship among the nanoparticle volume fraction, the pH of the suspension and the temperature gradient between the hot and the cold plate is investigated to identify any stability related issues. Finally, a thorough discussion on the findings is included to provide some future guidelines for effective nanofluids.

A. Thermophysical properties of nanofluids

For the calculation of the thermophysical properties of nanofluids, widely available empirical correlations and formulas from the literature were used, whereas, for DI water, they were obtained from Rohsenow et al. [34]. Also, the properties of both DI water and nanofluids were considered at the mean temperature of the hot and cold plates. For the density of nanofluids, ρ_{nf}, a well-accepted formula which relates the density of the base fluid, ρ_w, with the density and the volume fraction of the nanoparticles, ρ_n and φ, respectively was employed:

$$\rho_{nf} = (1-\varphi)\rho_w + \varphi\rho_n \quad (2)$$

As for the heat capacity of nanofluids $c_{p,nf}$, it was found through an extensively used correlation:

$$c_{p,nf} = \frac{\varphi\rho_n c_{p,p} + (1-\varphi)\rho_w c_{p,w}}{(1-\varphi)\rho_w + \varphi\rho_n} \quad (3)$$

For the nanofluid viscosity, μ_{nf}, two different formulas were used according to the averaged particle size confirmed by the TEM measurements. For the nanofluids synthesized with the Sigma Aldrich nanopowder, an empirical formula for nanoparticles with an average particle diameter of 20 nm and room temperature was employed that was also used by Maiga et al. [35] and Ni et al. [10]. The following formula gives good representation over a wide range of temperatures.

$$\mu_{nf} = \mu_w(1 + 7.3\varphi + 123\varphi^2) \quad (4)$$

For the nanofluids synthesized with the Alfa Aesar nanopowder, Eq. 4 was also used. As it was reported by Ni et al. [10], this formula gives also a reasonably good representation for a particle size of 131.2 nm, which is much bigger than ours.

Finally, for the conductivity, k_{nf}, a formula used by Ni et al. [10] was involved that has been evaluated with different Al_2O_3 – H_2O nanofluid data sets over comparable ranges of temperature, nanoparticle concentration and particle size.

$$k_{nf} = k_w[1 + (-49.796 + 0.178T)\varphi + (535.576 - 1.840T)\varphi^2] \quad (5)$$

In natural convection, the heat transfer correlations are of the form of $Nu = f(Gr, \mathrm{Pr})$. *Nu, Gr and Pr* are given by:

$$Nu = \frac{hL}{k} \quad (6)$$

$$Gr = \frac{g\beta\Delta T L^3}{\nu^2} \quad (7)$$

$$\mathrm{Pr} = \frac{\nu}{\alpha} \quad (8)$$

Finally, the product of the *Gr* and *Pr* numbers is known as Rayleigh number, which is given by,

$$Ra = \frac{g\beta\Delta T L^3}{\nu\alpha} \quad (9)$$

At steady state conditions, it is assumed that the temperature at the heating and cooling plates is uniform due to the highly conductive material of the aluminum plates and the insulation Teflon plates that surround them. Thus, the heat diffusion equation was adopted to calculate the surface temperatures Thu and Tcl:

$$T_{hu} = T_h - \frac{q'' d_{pth-hu}}{k_{pl}} \quad (10)$$

$$T_{cl} = T_c + \frac{q'' d_{pth-cl}}{k_{pl}} \quad (11)$$

Therefore, the heat transfer coefficient is given by,

$$h = \frac{q''}{(T_{hu} - T_{cl})} \quad (12)$$

B. Influence of nanoparticle volume fraction on heat transfer properties

In this work, DI water and Al_2O_3 – DI H_2O nanofluid experiments were conducted under turbulent natural convection, $Ra \sim 10^9$, for a range of nanoparticle volume fraction from 0.03 to 0.12 %. The imposed boundary conditions in the experiments were constant heat flux, corresponding to 125 W power input from the heating plate and constant temperature of 23 °C (average value) at the cold plate. For all three sets of nanofluid samples, the heat transfer parameters along with the boundary conditions of the study are presented in Table 1.

In Figure 4, the heat transfer coefficient under natural convection as a function of the nanoparticle volumetric concentration is illustrated. It can be clearly seen that the addition of aluminum oxide nanoparticles decreases, in general, the heat transfer performance of the carrier fluid under natural convection for the conditions of this study. First of all, concerning the sample A, the decrease observed is quite intense. Also, as the nanoparticle concentration increases, the heat transfer coefficient decreases in a linear trend. For the sample B, the decrease of the heat transfer coefficient is significantly less than sample A. Over the nanoparticle volume fraction range of this study, the heat transfer coefficient of the nanofluid remains constant and slightly lower than that of the base fluid, revealing minor decrease within the experimental uncertainty. Finally, for the third sample of nanofluid, sample C, similar behavior with the acidic nanofluid sample B is noticed. There is also a decreasing trend of the natural convective heat transfer performance, but still within the bounds of the experimental uncertainty. In Figure 5, the temperature gradient between the hot and cold plate as a function of the nanoparticle volumetric concentration is illustrated. It can be noticed that for the sample A, the temperature difference between the plates increases linearly

with the nanoparticle concentration, whereas for the samples B and C, the increase of the temperature gradient is not significant (< 2 %).

Table 1. Experimental conditions and thermophysical properties for DI water and nanofluid of various nanoparticle volume fractions.

sample	contents	φ vol. %	ΔT (°C)	h (W/m²K)	Nu	Pr	Ra (x10^9)
	DI water	0.00	52.27	374	58.2	3.6	2.7
A	DI water, Sigma Aldrich nanopowder	0.03	54.15	361	56.3	3.7	2.6
		0.06	55.26	353	54.9	3.7	2.7
		0.12	57.05	342	53.3	3.7	2.7
B	DI water, Sigma Aldrich nanopowder, acetic acid	0.03	52.87	369	57.3	3.5	2.8
		0.06	52.66	371	57.4	3.5	2.7
		0.12	52.99	369	56.9	3.5	2.7
C	DI water, Alfa Aesar nanopowder	0.03	52.36	373	57.9	3.5	2.7
		0.06	53.22	367	56.8	3.5	2.8
		0.12	53.34	366	56.4	3.5	2.8

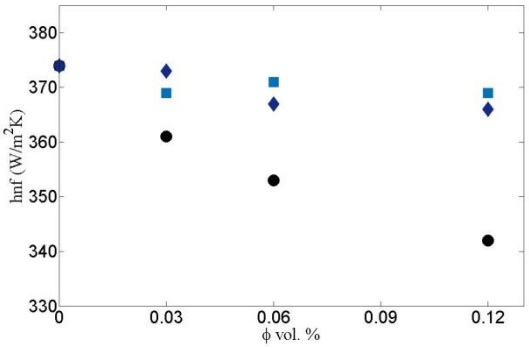

Figure 4. Convective heat transfer coefficient of the nanofluid as a function of nanoparticle volumetric concentration for different nanofluid samples of Table 1; A (circles), B (squares) and C set (rhombus).

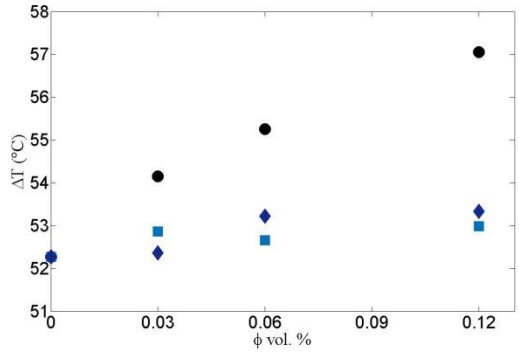

Figure 5. Temperature gradient between hot and cold plate as a function of nanoparticle volumetric concentration for the three nanofluid samples of Table 1; A (circles), B (squares) and C set (rhombus).

C. Influence of pH value on nanofluid stability

Considering the relationship among the reduction of the heat transfer coefficient, the increase of the temperature at the hot plate and the nanoparticle concentration in the base fluid, it seems that the degradation of the heat transfer that is experimentally observed is linked with the stability of the nanofluid. The quality of a nanofluid in terms of stability is related to its electrokinetic properties, as high surface charge of the dispersed particles results in strong repulsive forces among them. The first set of nanofluid samples contains no pH adjuster, thus its pH value depends on the properties of the dispersed nanoparticles and the quality of the DI water. In this study, high purity DI water, grade 3 (ISO 3696 standard), produced by distillation and capacitive deionisation was used. It had a pH value of 6.9 at the filling process, but due to the presence of CO_2 in the atmosphere and the addition of Al_2O_3 nanoparticles, the final pH of the suspension was expected to be different. Concerning the first sample (A), the pH of the synthesized nanofluid was measured at 8, very close to the IEP of γ-Al_2O_3. Therefore, the dispersed nanoparticles exhibited low surface charge and thus the electrostatic repulsion forces among them were weak. As a consequence, the propensity of the dispersed particles was to come closer to each other, form agglomerates and eventually settle. The poor quality of the nanofluid was qualitatively assessed at the end of an experiment, while the nanofluid was pumped out of the chamber. Figure 6(a) shows photographs of the deposition of nanoparticles and agglomerates at the surface of the heating plate of the chamber for a maximum nanoparticle volume fraction of 0.12 %.

For the second set of nanofluid samples, the pH of the suspension was adjusted by adding a small amount (< 0.0005 vol. %) of acetic acid with an assay ≥ 99.85 % to the base fluid. The average pH of the nanofluid was adjusted to 4.9 (at 50 °C), so as to be reasonably away from the IEP of aluminum oxide. Figure 6(b) depicts the deposition of the nanoparticles at the bottom of the chamber for the same nanoparticle volume fraction as before (0.12 %). It can be noticed that the fouling of the heating surface is less intense, indicating an improved quality of the synthesised nanofluid in terms of stability. This enhanced stability was also depicted by the limited temperature rise of the heating plate at steady state conditions. Finally, for the third set of samples, the nanopowder resulted in an acidic dispersion with an average pH value of 4.5 (at 50 °C). Figure 6(c) illustrates minor fouling of the bottom of the chamber with nanoparticles and agglomerates that led to a slight temperature increase at the heating plate, indicating that the nanofluid was physically stable.

D. Discussion

The addition of Al_2O_3 nanoparticles to pure DI H_2O was found to decrease the natural convective heat transfer performance under the specific experimental conditions. This result is consistent with most experimental studies in the literature, where the heat transfer coefficient, *h* and *Nu* decrease with the addition of nanoparticles. This finding comes in contrast to the common expectation that the heat transfer in nanofluids increases, as supported by many experimental investigations that deal with conduction, forced convection, boiling and critical heat flux. In addition, there are some numerical studies that simulate the behavior of nanofluids under natural convection that also report heat transfer

enhancement. A summary of some widely discussed mechanisms that could be responsible for any alteration of the heat transfer performance of nanofluids can be found in the extended literature review by Sergis and Hardalupas [4], even though there is no conclusive experimental evidence to support them at the time of writing this study. Additional reference can be found in a numerical study of the same authors [36], where the presence of a new type of complex heat transfer mechanism is addressed. In a previous study of the current authors [13], the decrease of the heat transfer coefficient under natural convection was attributed to the formation of a thin stationary layer structure that consists of nanoparticles, agglomerates and water molecules close to the heating surface. This work goes one step further as the electrostatic stabilization method was involved to eliminate the layer formation. More specifically, in the case of a pure nanofluid, with no pH controller involved, as the nanoparticle concentration increases, the fouling of the heating surface was more intense. Therefore, the temperature gradient in the chamber was increased and the heat transfer coefficient was decreased. This behaviour is attributed to the inadequacy of the system forces to ensure good nanofluid stability, in the absence of any pH changer or surfactant. However, once the electrostatic stabilization method was involved, the thickness of the thin layer structure close to the hot plate was qualitatively observed to reduce. The same resulted for the nanofluid whose dispersed nanoparticles exhibit acidic surface properties. In both sets of samples, the temperature at the heating plate did not significantly increase and thus the reported heat transfer decrease was minor. This is credited to the pH of the suspensions that were far away from the IEP of aluminium oxide. As a consequence, the dispersed nanoparticles exhibited high surface charge that led to strong electrostatic repulsion forces among them. Therefore, in cases where low-velocity applications are concerned, special attention should be paid to produce homogenous and stable dispersion of the powder in the liquid phase, as the buoyant and gravitational forces acting in the system appear to be inadequate to ensure good stability. Hence, the electrokinetic stabilization method or the proper selection of a nanopowder in terms of material, physical characteristics and manufacturing process can help towards this direction.

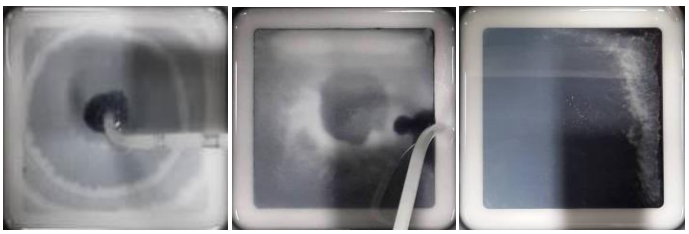

(a) (b) (c)

Figure 6. Top view of the fouling of the heating surface observed when pumping the 0.12 vol. % nanofluid out of the rig, at the end of the experiment for the (a) A, (b) B and (c) C sample.

CONCLUSIONS

This experimental study addresses the heat transfer characteristics of Al_2O_3 – DI H_2O nanofluids under turbulent natural convection, with and without using the electrostatic stabilization method during the preparation of the nanofluids. Heat transfer measurements were obtained in a classical Rayleigh-Benard configuration and compared with pure DI water results. Our findings show that, under the specific operating conditions, the addition of aluminium nanoparticles to the aqueous base fluid decreases the heat transfer performance. In the case of a pure nanofluid, where no pH adjuster or dispersant was involved, the deterioration increased with the nanoparticle concentration. This was a first indication of poor nanofluid stability that led to the fouling of the heating plate with nanoparticles and large agglomerates. On the contrary, the effect of the electrostatic stabilization method led to superior nanofluid stability by simply altering the concentration of ions in the system. Therefore, by adjusting the pH of the nanofluid reasonably away from the IEP of aluminium oxide, the nanoparticles exhibit high surface charge that results in strong repulsive forces among them. The same result was obtained when nanopowder that exhibits acidic behaviour in DI water was used, that resulted in a nanopowder dispersion with a pH value similar to that obtained by adjusting the pH as mentioned above but without the addition of any pH changer. Up to date, there is not a single, ideal pH for nanofluids addressed in the literature, as this is a compromise of many different factors, namely the physical characteristics of the nanoparticles, the manufacturing process that is followed, the quality of the base fluid, the presence of dispersants, the preparation method of the nanofluid and the application involved. To summarise, when low-velocity flows or stationary nanofluids are involved, special attention should be paid to ways of improving the stability of the nanofluid by involving methods such as the electrostatic stabilization or the steric stabilisation as a next step. However, further investigation is required to ensure the quality of the resulting nanofluid under the operating conditions of the study and to prevent any possible damage to the components of the system involved. Finally, a more systematic approach needs to be followed when nanofluid results are presented or compared, as the pH of a suspension appears to be a key factor that should be taken into consideration. It can be clearly understood that the pH of a nanofluid and the corresponding surface charge of the nanoparticles do not only affect the dispersion or aggregation of the particles. They do control the final average particle size in the suspension and subsequently the heat transfer behavior, along with the macroscopic and microscopic heat and mass transfer mechanisms involved.

REFERENCES

[1] J. Milnes, A. Burns, D. Drikakis, Computational modelling of the HyperVapotron on cooling technique, Fusion Engineering and Design, 87(9) (2012) 1647-1661.

[2] S.U.S. Choi, Nanofluids: from vision to reality through research, Journal of Heat Transfer, 131(3) (2009) 1–9.

[3] Y. Li, J.e. Zhou, S. Tung, E. Schneider, S. Xi, A review on development of nanofluid preparation and characterization, Powder Technology, 196(2) (2009) 89-101.
[4] A. Sergis, Y. Hardalupas, Anomalous heat transfer modes of nanofluids: a review based on statistical analysis, Nanoscale Research Letters, 6(1) (2011) 391-391.
[5] D. Wen, G. Lin, S. Vafaei, K. Zhang, Review of nanofluids for heat transfer applications, Particuology, 7(2) (2009) 141-150.
[6] Y. Xuan, Q. Li, Investigation on convective heat transfer and flow features of nanofluids, Journal of Heat Transfer, 125(1) (2003) 151-155.
[7] A.K. Nayak, M.R. Gartia, P.K. Vijayan, An experimental investigation of single-phase natural circulation behavior in a rectangular loop with Al_2O_3 nanofluids, Experimental Thermal and Fluid Science, 33(1) (2008) 184-189.
[8] S. Kakaç, A. Pramuanjaroenkij, Review of convective heat transfer enhancement with nanofluids, International Journal of Heat and Mass Transfer, 52(13-14) (2009) 3187-3196.
[9] D. Wen, Y. Ding, Formulation of nanofluids for natural convective heat transfer applications, International Journal of Heat and Fluid Flow, 26(6) (2005) 855-864.
[10] R. Ni, S.-Q. Zhou, K.-Q. Xia, An experimental investigation of turbulent thermal convection in water-based alumina nanofluid, Physics of Fluids, 23(2) (2011) 022005.
[11] N. Putra, W. Roetzel, S.K. Das, Natural convection of nano-fluids, Heat and Mass Transfer, 39 (2003) 775-784.
[12] C.H. Li, G.P. Peterson, Experimental studies of natural convection heat transfer of Al_2O_3/DI water nanoparticle suspensions (nanofluids), Advances in Mechanical Engineering, 2 (2010) 742739.
[13] K. Kouloulias, A. Sergis, Y. Hardalupas, Sedimentation in nanofluids under a natural convection experiment, International Journal of Heat and Mass Transfer-submitted, (2016).
[14] K. Khanafer, K. Vafai, M. Lightstone, Buoyancy-driven heat transfer enhancement in a two-dimensional enclosure utilizing nanofluids, 46 (2003) 3639-3653.
[15] H.F. Oztop, E. Abu-Nada, Numerical study of natural convection in partially heated rectangular enclosures filled with nanofluids, International Journal of Heat and Fluid Flow, 29(5) (2008) 1326-1336.
[16] S.M. Aminossadati, B. Ghasemi, Natural convection cooling of a localised heat source at the bottom of a nanofluid-filled enclosure, European Journal of Mechanics, B/Fluids, 28(5) (2009) 630-640.
[17] N. Ben-Cheikh, A.J. Chamkha, B. Ben-Beya, T. Lili, Natural convection of water-based nanofluids in a square enclosure with non-uniform heating of the bottom wall, Journal of Modern Physics, 04(02) (2013) 147-159.
[18] A. Ghadimi, R. Saidur, H.S.C. Metselaar, A review of nanofluid stability properties and characterization in stationary conditions, International Journal of Heat and Mass Transfer, 54(17-18) (2011) 4051-4068.
[19] V. Trisaksri, S. Wongwises, Nucleate pool boiling heat transfer of TiO_2–R141b nanofluids, International Journal of Heat and Mass Transfer, 52(5-6) (2009) 1582-1588.
[20] S.U. Ilyas, R. Pendyala, N. Marneni, Preparation, sedimentation, and agglomeration of nanofluids, Chemical Engineering & Technology, 37(12) (2014) 2011-2021.
[21] D. Wen, Y. Ding, Formulation of nanofluids for natural convective heat transfer applications, International Journal of Heat and Fluid Flow, 26 (2005) 855-864.
[22] D. Wen, Y. Ding, Experimental investigation into the pool boiling heat transfer of aqueous based γ-alumina nanofluids, Journal of Nanoparticle Research, (7) (2005) 265-274.
[23] J.A. Eastman, S.U.S. Choi, S. Li, W. Yu, L.J. Thompson, Anomalously increased effective thermal conductivities of ethylene glycol-based nanofluids containing copper nanoparticles, Applied Physics Letters, 78(6) (2001) 718.
[24] C. Mao, H. Zou, X. Zhou, Y. Huang, H. Gan, Z. Zhou, Analysis of suspension stability for nanofluid applied in minimum quantity lubricant grinding, The International Journal of Advanced Manufacturing Technology, 71(9-12) (2014) 2073-2081.
[25] B.C. Pak, Y. Cho, Hydrodynamic and heat transfer study of dispersed fluids with submicron metallic oxide particles, Experimental Heat Transfer, 11(2) (1998) 151-170.
[26] B.P. Singh, R. Menchavez, C. Takai, M. Fuji, M. Takahashi, Stability of dispersions of colloidal alumina particles in aqueous suspensions, Journal of Colloid and Interface Science, 291(1) (2005) 181-186.
[27] S. Mukherjee, S. Paria, Preparation and stability of nanofluids-a review, IOSR Journal of Mechanical and Civil Engineering, 9(2) (2013) 63-69.
[28] S. Adegbite, Particle characterisation and grinding behaviour of gamma-alumina slurries prepared in a stirred media mill, Journal of Materials Science Research, 2(1) (2012) 135-147.
[29] J.-H. Lee, K.S. Hwang, S.P. Jang, B.H. Lee, J.H. Kim, S.U.S. Choi, C.J. Choi, Effective viscosities and thermal conductivities of aqueous nanofluids containing low volume concentrations of Al_2O_3 nanoparticles, International Journal of Heat and Mass Transfer, 51(11-12) (2008) 2651-2656.
[30] D. Wen, Y. Ding, Natural convective heat transfer of suspensions of titanium dioxide nanoparticles (nanofluids), IEEE Transactions on Nanotechnology 5(3) (2006) 220-227.
[31] T.R. Barrett, S. Robinson, K. Flinders, A. Sergis, Y. Hardalupas, Investigating the use of nanofluids to improve high heat flux cooling systems, Fusion Engineering and Design, 88(9-10) (2013) 2594-2597.
[32] H. Zhu, C. Li, D. Wu, C. Zhang, Y. Yin, Preparation, characterization, viscosity and thermal conductivity of $CaCO_3$ aqueous nanofluids, Science China Technological Sciences, 53(2) (2010) 360-368.
[33] L. Kirkup, Experimental methods; an introduction to the analysis and presentation of data, John Wiley & Sons Australia, Ltd, 1994.
[34] W.M. Rohsenow, J.P. Hartnett, Y.I. Cho, Handbook of Heat Transfer, third edition, McGraw-Hill, 1998.
[35] S.E.B. Maïga, C.T. Nguyen, N. Galanis, G. Roy, Heat transfer behaviours of nanofluids in a uniformly heated tube, Superlattices and Microstructures, 35(3-6) (2004) 543-557.
[36] A. Sergis, Y. Hardalupas, Revealing the complex conduction heat transfer mechanism of nanofluids, Nanoscale Research Letters, 10(1) (2015) 954.